Alpha satellite insertions and the evolutionary landscape of centromeres

Giuliana Giannuzzi[1,2,3], Glennis A. Logsdon[4], Nicolas Chatron[3,5,6], Danny E. Miller[4,7], Julie Reversat[5], Katherine M. Munson[4], Kendra Hoekzema[4], Marie-Noëlle Bonnet-Dupeyron[8], Pierre-Antoine Rollat-Farnier[5,9], Carl A. Baker[4], Damien Sanlaville[5,6], Evan E. Eichler[4,10], Caroline Schluth-Bolard[5,6], Alexandre Reymond[3]

1. Department of Biosciences, University of Milan, Milan, Italy
2. Institute of Biomedical Technologies, National Research Council, Milan, Italy
3. Center for Integrative Genomics, University of Lausanne, Lausanne, Switzerland
4. Department of Genome Sciences, University of Washington School of Medicine, Seattle, WA, USA
5. Service de génétique, Hospices Civils de Lyon, Lyon, France
6. Institut NeuroMyoGène, University of Lyon, Lyon, France
7. Department of Pediatrics, Division of Genetic Medicine, University of Washington and Seattle Children's Hospital, Seattle, WA, USA
8. Service de Cytogénétique, Centre Hospitalier de Valence, Valence, France
9. Cellule Bioinformatique, Hospices Civils de Lyon, Lyon, France
10. Howard Hughes Medical Institute, University of Washington, Seattle, WA 98195, USA

Correspondence to:

Giuliana Giannuzzi
University of Milan
Department of Biosciences
Via Giovanni Celoria, 26
20133 Milano, Italy
giuliana.giannuzzi@unimi.it

Abstract

Human centromeres are composed of alpha satellite DNA hierarchically organized as higher-order repeats and epigenetically specified by CENP-A binding. Current evolutionary models assert that new centromeres are first epigenetically established and subsequently acquire an alphoid array. We identified during routine prenatal aneuploidy diagnosis by FISH a *de novo* insertion of alpha satellite DNA array (~50-300 kbp) from the centromere of chromosome 18 (D18Z1) into chromosome 15q26 euchromatin. Although bound by CENP-B, this locus did not acquire centromeric functionality as demonstrated by lack of constriction and absence of CENP-A binding. We characterized the rearrangement by FISH and sequencing using Illumina, PacBio, and Nanopore adaptive sampling which revealed that the insertion was associated with a 2.8 kbp deletion and likely occurred in the paternal germline. Notably, the site was located ~10 Mbp distal from the location where a centromere was ancestrally seeded and then became inactive sometime between 20 and 25 million years ago (Mya), in the common ancestor of humans and apes. Long reads spanning either junction showed that the organization of the alphoid insertion followed the 12-mer higher-order repeat structure of the D18Z1 array. Mapping to the CHM13 human genome assembly revealed that the satellite segment transposed from a specific location of chromosome 18 centromere. The rearrangement did not directly disrupt any gene or predicted regulatory element and did not alter the epigenetic status of the surrounding region, consistent with the absence of phenotypic consequences in the carrier. This case demonstrates a likely rare but new class of structural variation that we name 'alpha satellite insertion'. It also expands our knowledge about the evolutionary life cycle of centromeres, conveying the possibility that alphoid arrays can relocate near vestigial centromeric sites.

Introduction

Alpha satellite is a class of highly repetitive DNA defined by a group of related, highly divergent AT-rich repeats or 'monomers', each approximately 171 bp in length. Alpha satellite, also named alphoid DNA, comprises up to 10% of the human genome and is mostly found tandemly repeated within constitutive heterochromatin at centromeres and pericentromeric regions. At centromeric regions, satellite monomers are hierarchically organized into larger repeating units, in which a defined number of monomers have been homogenized. These units, which are named 'higher-order repeats' (HORs), are tandemly arranged into chromosome-specific, megabase-sized satellite arrays with limited nucleotide differences between repeat copies (Willard and Waye 1987; Durfy and Willard 1989; Schueler et al. 2001; McNulty and Sullivan 2018; Miga et al. 2020).

The centromere is the chromosomal locus where sister chromatids attach and the kinetochore is assembled, which is essential for proper chromosome segregation during cell division. While alpha satellite DNA constitutes the sequence of all mature centromeres, it is not sufficient nor necessary for centromere identity. This is demonstrated by dicentric chromosomes that assemble the kinetochore at only one of two alpha-satellite regions (Earnshaw and Migeon 1985) and analphoid chromosomes that possess fully functional centromeres (Voullaire et al. 1993). Centromere function appears to be epigenetically established and maintained by local enrichment of the CENP-A histone H3 variant within nucleosomes rather than presence of alphoid DNA (Palmer et al. 1991; Karpen and Allshire 1997; Panchenko and Black 2009; McKinley and Cheeseman 2016). This function can be inactivated at an original site and moved to a new position along the chromosome (Montefalcone et al. 1999). It is similarly turned off after a chromosomal fusion to ensure stability of the derived dicentric chromosome. These events determine the emergence of evolutionary new centromeres and the appearance of recognizable genomic regions where the centromere used to be positioned in the past (Amor and Choo 2002; Rocchi et al. 2009). Insights into the molecular steps of centromere repositioning from the birth of a new centromere to its maturity were uncovered by studying fly, primate, and equid chromosomes (Marshall et al. 2008; Piras et al. 2010). These analyses showed that new centromeres are first epigenetically specified and then mature by acquiring the satellite DNA array, in some cases going through intermediate configurations bearing DNA amplification (Kalitsis and Choo 2012; Nergadze et al. 2018).

Besides the main pericentromeric and centromeric locations, smaller regions of alpha satellite DNA are located in the euchromatin of the human genome, >5 Mbp from the centromeres, with

around 100 blocks annotated in the reference by the RepeatMasker program (Rudd and Willard 2004; Feliciello et al. 2020). For example, three large blocks, respectively 11, 8, and 13 kbp long, are located within cytoband 2q21 with SVA (SINE/VNTR/Alu) and LINE elements intervening between them. These alphoid sequences are the relics of an ancestral centromere that became inactive ~5 Mya after the fusion of two ancestral chromosomes in the human lineage compared to big apes (IJdo et al. 1991; Avarello et al. 1992; Baldini et al. 1993; Chiatante et al. 2017).

Here, we report an individual with a *de novo* insertion of an alpha satellite DNA array from the centromere of chromosome 18 into chromosome 15q26, the first observation of insertion of satellite DNA array into the euchromatin of the human genome that we are aware of. This case brings to light a probably rare and new class of structural variation and expands our knowledge on the evolutionary life cycle of centromeres and the origin and spread of alpha satellite in primate genome.

Results

Prenatal, postnatal and family investigations

Amniocentesis was performed at 15 weeks' gestation in a 35 years-old gravida 6 para 2 woman. She already had two healthy children, one miscarriage, and two pregnancies terminated due to fetal trisomy 21. Interphase FISH (Fluorescent *In Situ* Hybridization) on uncultured amniocytes with probes for main aneuploidies showed the presence of three signals for the alpha satellite DNA probe of chromosome 18 (D18Z1) in all cells (150/150) and three signals for chromosome 21 specific probes in 29 out of 121 cells (24%), suggesting a trisomy 18 and a mosaic trisomy 21. Karyotyping of cultured cells confirmed the presence of the mosaic trisomy 21 at 19% (12/62 cells) but showed the presence of two normal chromosomes 18. Metaphase FISH on cultured cells revealed the aberrant hybridization of the D18Z1 probe at chromosome 15q26 (**Figure 1A**). The intensity and size of the FISH signal suggested that the length of the inserted satellite DNA was ~50-300 kbp. Chromosomal microarray did not show any imbalances, except the mosaic trisomy 21 (13%). FISH analysis of both parents showed that the alphoid DNA insertion was *de novo*. Pregnancy sonographic follow-up was normal. The proband, a healthy male baby, was born at term with normal birth parameters. Post-natal karyotype and FISH confirmed the mosaic trisomy 21 (6/33 cells; 18%) and the presence of the insertion of chromosome 18 alpha satellite on the long arm of a chromosome 15. At one

115 year old, growth clinical examination (weight 10.6 kg, +1 standard deviation (SD); height 75
116 cm, +1 SD; occipito-frontal circumference 46.5 cm, +1SD) and psychomotor development
117 were normal, consistent with low level mosaic trisomy 21 and also suggesting that the alpha
118 satellite insertion had no phenotypic consequences.

119

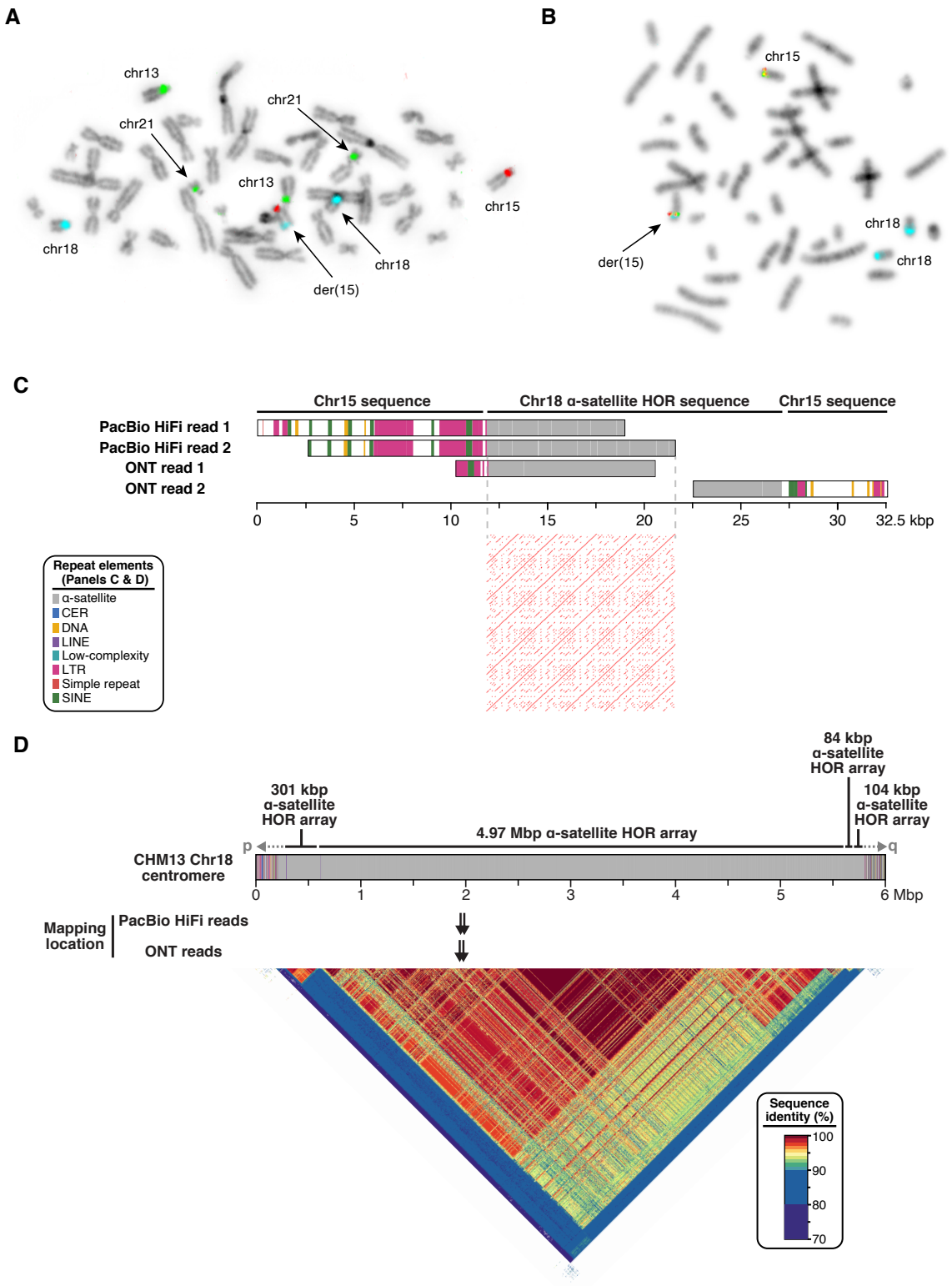

Figure 1. D18Z1 alpha satellite *de novo* insertion. **A)** FISH results of cultured amniocytes using alpha satellite DNA probes of chromosomes 15 (D15Z1, Texas-Red), 13/21 (D13/21Z1, green), and 18 (D18Z1, aqua) probes. **B)** FISH results of cultured amniocytes using the 15q25 BAC probes RP11-635O8 (red) and RP11-752G15 (green) flanking the ancestral centromere, and the D18Z1 (aqua) probe. **C)** Read length, repeat composition (color code in inset), and mapping location of the four selected HiFi and ONT reads (*top*). Dot plot (window size 20) of the longest available alpha satellite sequence (*bottom*). **D)** Schematic representation of the CHM13-T2T

127 chromosome 18 centromere with its repeat composition (*top*). A heatmap representation of sequence identity over
128 the region is presented below. The mapping location of the PacBio HiFi and ONT reads is pinpointed by black
129 arrows.

130

131 *Structural characterization of the rearrangement*

132 To characterize the alphoid DNA insertion at the sequence level, we performed WGS (whole
133 genome sequencing) of the proband using the short-read Illumina platform. We first analyzed
134 these data using a routine clinical analysis pipeline that did not identify any structural variant
135 at chromosome 15q26. We then followed a customized approach, mapping reads to a library
136 made up of the entire chromosome 15 and chromosome 18 centromeric alpha satellite DNA
137 sequences. We isolated high-quality discordant paired reads mapped to both sequences, as well
138 as chimeric reads anchored to chromosome 15 and containing alpha satellite DNA. These reads
139 allowed us to define the positions of the proximal and distal breakpoints of the insertion at
140 chr15:92,359,068 and chr15:92,361,920 (GRCh38), respectively. These coordinates, both
141 subsequently validated by PCR, revealed the deletion of a 2,851 bp segment that was replaced
142 by the insertion. We noted that the target site was ~10 Mbp distal from the position where an
143 ancestral centromere was seeded and was shown to be active ~25 Mya in the common ancestor
144 of Old World monkeys and apes, and was then inactivated sometime between 20 and 25 Mya
145 in the common ancestor of the Hominoids (lesser apes, great apes, and humans) (Ventura et al.
146 2003). This was further confirmed by the co-hybridization of the D18Z1 probe with two BAC
147 probes flanking the ancestral centromere locus (RP11-752G15 and RP11-635O8) (Giannuzzi
148 et al. 2013). This experiment showed, at metaphase resolution, that the satellite probe signal
149 colocalized with both BAC probes on the derivative chromosome 15 (**Figure 1B**).

150 We then sought to better characterize the rearrangement by generating long-read sequence
151 information. We employed two technologies, ONT (Oxford Nanopore Technologies) with
152 selective sampling via Read Until (Loose et al. 2016), targeting 50 kb of sequence on either
153 side of the insertion, and PacBio HiFi sequencing. We sequenced the proband (~11.5x coverage
154 at the targeted region), father (~20.1x), and mother (~19.8x) using readfish (Payne et al. 2020)
155 on an ONT GridION, and the proband's genome on one PacBio SMRT cell (~6.5x coverage).
156 We confirmed the insertion breakpoints and the 2.8 kbp deletion but were unable to assemble
157 a contiguous sequence spanning the entire insertion. To determine which parental chromosome
158 the event occurred on, we phased the proband, father, and mother's ONT reads and searched
159 for diagnostic single-nucleotide variants that differed between the maternal and paternal

160 haplotypes. The proband is hemizygous for two maternal variants mapping within the deleted
161 region while the father is homozygous for the alternative allele. Conversely, the proband
162 harbored one paternal variant on the haplotype with the insertion that is absent in his mother.
163 This demonstrated that the rearrangement occurred on the paternal chromosome. Analysis of
164 the junctions showed that, besides the aforementioned deletion, no further rearrangements,
165 such as a target site duplication, occurred at the boundaries. At the proximal junction, a short
166 sequence stretch of four nucleotides (CAAA) was identified that could not uniquely be
167 assigned to the chromosome 15 or the satellite DNA. However, due to its small size, it is
168 unlikely that this stretch of homologous sequence had a role in the rearrangement mechanism,
169 particularly in the determination of the target site.

170 We analyzed the content of interspersed repeats in 5 kb segments upstream and downstream of
171 the rearrangement breakpoints as well as in the deleted segment on chromosome 15 sequence.
172 These segments were enriched for LTR (long terminal repeats derived from endogenous
173 retroviruses) content when compared to the human genome average, as assessed by simulation
174 for the entire 13 kb segment (4.34-fold, $P = 0.035$, **Table 1**).

175

176 **Table 1. Content in interspersed repeat elements of the rearranged target site on chromosome 15.** The "*E*"
177 value is the enrichment coefficient that was calculated by dividing the observed value by the mean of 10,000
178 genome-wide permutations (human genome average).

	Sequence upstream of the insertion (5 kb)	Deletion (2851 bp)	Sequence downstream of the insertion (5 kb)	Entire region	Human genome average	*E*, *P* ± SE
SINEs	9%	0%	12%	8%	12%	0.65, 0.57 ± 0.005
LINEs	0%	0%	0%	0%	19%	0, 1
LTR elements	62%	32%	13%	36%	8%	4.34, 0.035 ± 0.002
DNA elements	0%	0%	9%	4%	3%	1.21, 0.3 ± 0.005

179

180 *Structural characterization of the alpha satellite DNA insertion*

181 While we were unable to assemble the full sequence of the insertion, we investigated its
182 structural properties by identifying reads with the longest content in alpha satellite DNA and
183 unequivocally derived from this site, i.e. chimeric reads anchored to chromosome 15 sequence
184 on either side of the insertion, spanning one breakpoint, and containing chromosome 18
185 centromeric alpha satellite sequences.

186 We selected two HiFi reads with estimated >99.9% accuracy and 7,199 bp (PacBio HiFi read
187 1) and 9,821 bp (PacBio HiFi read 2) of satellite DNA, both spanning the proximal junction;
188 an ONT read with 8,618 bp of satellite DNA at the proximal junction (ONT read 1); an ONT
189 read with 4,583 bp of satellite DNA at the distal junction (ONT read 2) (**Figure 1C**). Best
190 alignments to the human genome reference (GRCh38) of alpha satellite segments from these
191 four sequences showed identity with centromere reference models of chromosome 18 (Miga et
192 al. 2014; Rosenbloom et al. 2015). Alignments to the CHM13-T2T (Telomere-to-Telomere)
193 genome (Logsdon et al. 2020; Miga et al. 2020) resulted in unique locations for each read and
194 pointed the origin of the transposition to a precise 10 kbp region in the centromere of
195 chromosome 18 (chr18:17500487-17510699) (**Figure 1D**). While HiFi reads showed high
196 identity (99%) with this region, ONT reads showed lower values (94%), mainly due to errors
197 in their sequence. As the estimated size of the transposed segment (order of hundreds kbp) is
198 bigger than the size of the corresponding interval within chromosome 18 centromeric sequence,
199 we hypothesize that this region is likely expanded in the proband or alternatively in his paternal
200 lineage and, therefore, structurally different from the CHM13 centromere. Overall, these
201 results confirmed that the insertion originated from chromosome 18 centromeric DNA.

202 As chromosome 18 centromere is composed of two alpha satellite families, family I (D18Z1)
203 and family II (D18Z2), both belonging to the suprachromosomal family 2 (SF2), whose arrays
204 have a dimeric structure based on D1 and D2 monomers (Alexandrov et al. 1991), we assessed
205 the similarity with deposited sequences representing both families. Local pairwise alignments
206 showed 98% and 81% identity of both PacBio HiFi reads, respectively with D18Z1
207 (M65181.1) and D18Z2 (M38466.1) sequences, and 89.9% and 77.1% identity for the ONT
208 read 2 transitioning over the distal breakpoint. These results indicate a closer relationship of
209 the inserted satellite DNA to the D18Z1 family.

210 We analyzed the repetitive structure of the PacBio HiFi read 2, as it contains the longest
211 satellite array sequence. We used the re-DOT-able tool
212 (https://www.bioinformatics.babraham.ac.uk/projects/redotable/) and observed a higher
213 density of matches every ~2000 bp (**Figure 1C, *bottom panel***). To further assess this
214 periodicity, we extracted 57 monomers (size range 165-174 bp), built a multiple sequence
215 alignment, and visualized all pairwise identity percentages by creating two heatmaps. The first
216 one shows monomers ordered according to their position in the array, while the second heatmap
217 depicts monomers ordered according to the dendrogram determined by the hierarchical
218 clustering of identity percentages (**Figure 2A**). In the dendrogram-based heatmap, the

monomers cluster into two main groups as expected from the dimeric structure of the D18Z1 array (**Figure 2A**). D1-D1/D2-D2 sequence identity range from 78 to 100% (median 85%); D1-D2 identity range from 63 to 78% (median 70%) (**Figure 2B**). We then grouped every 12 monomers into ~2 kb units and obtained four repeats with 99.21-99.85% pairwise sequence identity (**Figure 2C**). These results are consistent with a 12-mer HOR structure, matching the known organization of the D18Z1 satellite array (McNulty and Sullivan 2018).

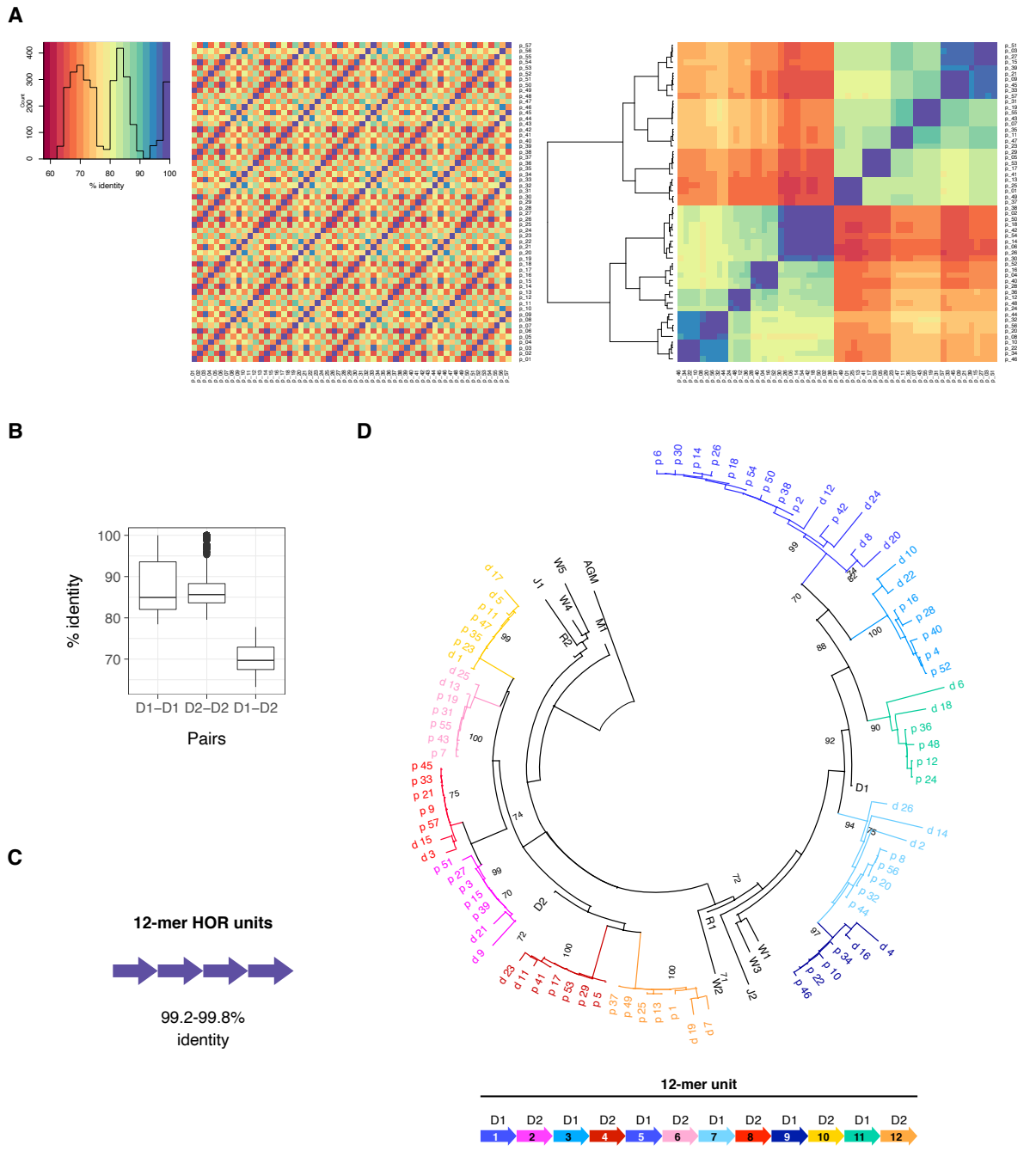

227 **Figure 2. Organization of the alpha satellite array. A)** Heatmaps of identity percentages between the 57 alpha
228 satellite monomers of ~171 bp derived from the PacBio HiFi read 2, with monomers ordered either according to
229 their position in the array (*left*) or as determined by clustering (*right*). **B)** Boxplots of identity percentages between
230 D1-D1, D2-D2, and D1-D2 monomer pairs. **C)** Identity percentages between 12-mer HOR units. **D)** (*top*)
231 Neighbor-joining tree of alphoid monomers from the PacBio HiFi read 2 transitioning over the proximal ('p')
232 junction and from the ONT read 2 transitioning over the distal ('d') junction with sequences of the 12 human
233 monomer types (D1, D2, J1, J2, M1, R1, R2, W1-5) and the alpha satellite from the African Green Monkey
234 (AGM) as outgroup. Monomers are numbered according to their position in the arrays. Bootstrap values >70 are
235 shown. (*bottom*) Schematic of the 12-mer HOR unit.

236

237 Finally, we extracted an additional 26 monomers (size range 158-177 bp) from the ONT read
238 2 spanning the distal breakpoint (in spite of the inherent sequencing uncertainties) and
239 multialigned all monomers with sequences of the 12 different monomer types (D1, D2, J1, J2,
240 M1, R1, R2, W1-5) found at all human centromeres and the alpha satellite sequence from the
241 African Green Monkey as an outgroup. Despite differences in the accuracy of HiFi and ONT
242 sequences, all monomers identified in the insertion clustered in two major clades formed by
243 D1 and D2 monomers, confirming the assignment to these two monomer types. D1 and D2
244 monomers further grouped into 11 clades in agreement with their organization in a HOR unit
245 of 12 monomers, with D1 monomers at positions 1 and 5 that were homogenized and formed
246 a single clade (**Figure 2D**).

247

248 *Functional profiling of the rearranged site*

249 To assess whether this structural change is likely to have functional impact, we examined gene
250 annotation (GENCODE v32) at the insertion breakpoints as well as in the deleted region. We
251 find that the rearrangement did not directly disrupt any gene, with the closest one (*ST8SIA2*)
252 annotated 32 kb distally (**Figure 3A**). We then evaluated whether the rearrangement affected
253 other functional elements, such as regulatory DNA. To this end, we leveraged publicly
254 available data from the ENCODE consortium of chromatin activity measured by chromatin
255 immunoprecipitation sequencing (ChIP-seq) for three histone modifications, i.e. methylated
256 histone 3 at lysine 4 (H3K4me1), tri-methylated histone 3 at lysine 4 (H3K4me3), and
257 acetylated histone 3 at lysine 27 (H3K27ac), on seven cell lines. These epigenetic marks are
258 associated with poised enhancers (H3K4me1), promoters (H3K4me3), and active enhancers
259 (H3K27ac). Neither the deleted segment nor the breakpoints overlapped any of these chromatin
260 features, suggesting that the rearrangement did not disrupt a regulatory element (**Figure 3A**).

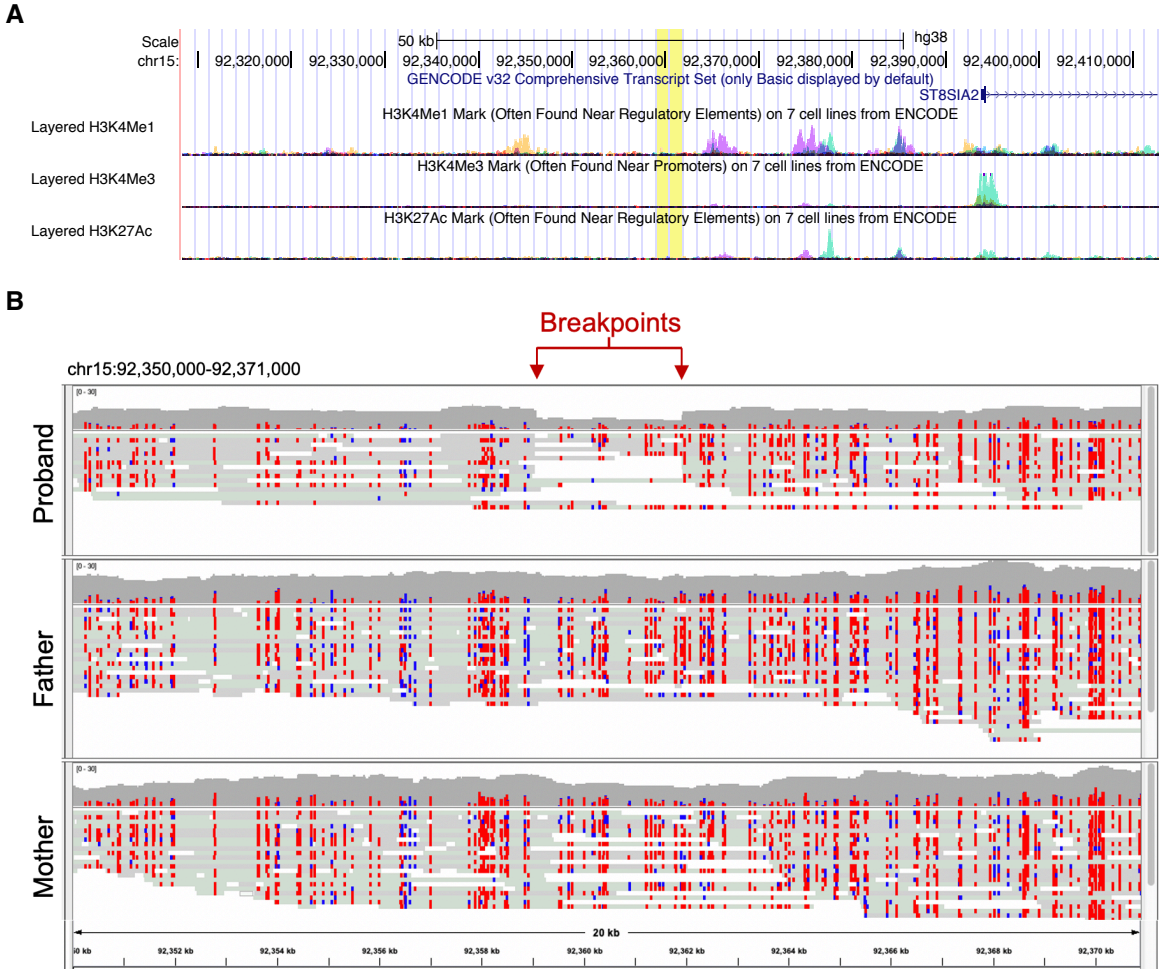

Figure 3. Functional profiling of the rearrangement site. A) UCSC view of the 100 kbp region surrounding the rearrangement at 15q26.1. The deleted region is highlighted in yellow, with deletion extremes corresponding to the satellite insertion positions. The GENCODE v32 and ENCODE regulations (H3K4me1, H3K4me3, and H3K27ac) tracks are shown (hg38). No gene and no enrichment of epigenetic marks found near regulatory elements are annotated in the deleted region. The closest gene, *ST8SIA2*, is mapped 32 kb distally. **B) Methylation pattern of the insertion site in the family trio**. Methylation data obtained from the ONT selective sequencing. Methylated (red) and unmethylated (blue) CpGs are shown. The methylation profiles are similar among the family trio.

Next, we assessed whether the insertion of centromeric satellite DNA, which comes from a heterochromatic locus, modifies the epigenetic status of the 15q26 target region. We leveraged CpG methylation data of the 20 kb genomic segment surrounding the insertion site using the ONT data of the proband and his parents. Cytosine methylation is an epigenetic modification often found in CpG dinucleotides that contributes to the formation of heterochromatic regions

277 and leads to transcriptional modulation, in particular silencing. Comparison of the proband
278 mutated allele with unrearranged ones, i.e. his maternal allele and the four alleles of his parents,
279 revealed no major difference in the methylation patterns, indicating that the satellite insertion
280 did not alter the methylation status of the surrounding region (**Figure 3B**). The absence of
281 functional elements (gene or likely regulatory element) at the site and the maintenance of the
282 methylation profile of the broader region suggest that the rearrangement itself has had no
283 functional consequences. This is in line with the absence of clinical features in the proband that
284 could not be explained by his trisomy 21 mosaicism.

285

286 *Immuno-FISH with anti CENP-A and CENP-B antibodies*

287 Cytogenetic evaluation of the derived chromosome 15 revealed no chromosomal constriction
288 at the position where the satellite DNA sequence was inserted, suggesting that this site did not
289 acquire properties of a functional centromere. To further demonstrate this lack of
290 epigenetically-defined centromeric function, we performed an immuno-FISH experiment with
291 an antibody against the CENP-A protein. We observe no colocalization of the D18Z1 probe
292 and CENP-A staining at the satellite insertion locus on the derivative chromosome 15 (**Figure**
293 **4**). We also assessed by immuno-FISH the binding of the CENP-B box by the CENP-B protein.
294 In 20 out of 25 mitoses, we observe a faint pattern of staining of the CENP-B antibody
295 corresponding to the satellite insertion, whereas in the remaining five we observed no signal
296 (**Figure 4**). Such faint signals may derive either from the smaller size of the satellite insertion
297 compared to a centromeric satellite array or to a weaker binding of the CENP-B protein.
298 Nevertheless, these results suggest that CENP-B proteins recognize and bind the CENP-B box
299 on the satellite monomers of the inserted sequence. Although CENP-B is not necessary and
300 sufficient to confer centromeric function, it was shown that it creates epigenetic chromatin
301 states permissive for CENP-A or heterochromatin assembly (Otake et al. 2020).

302

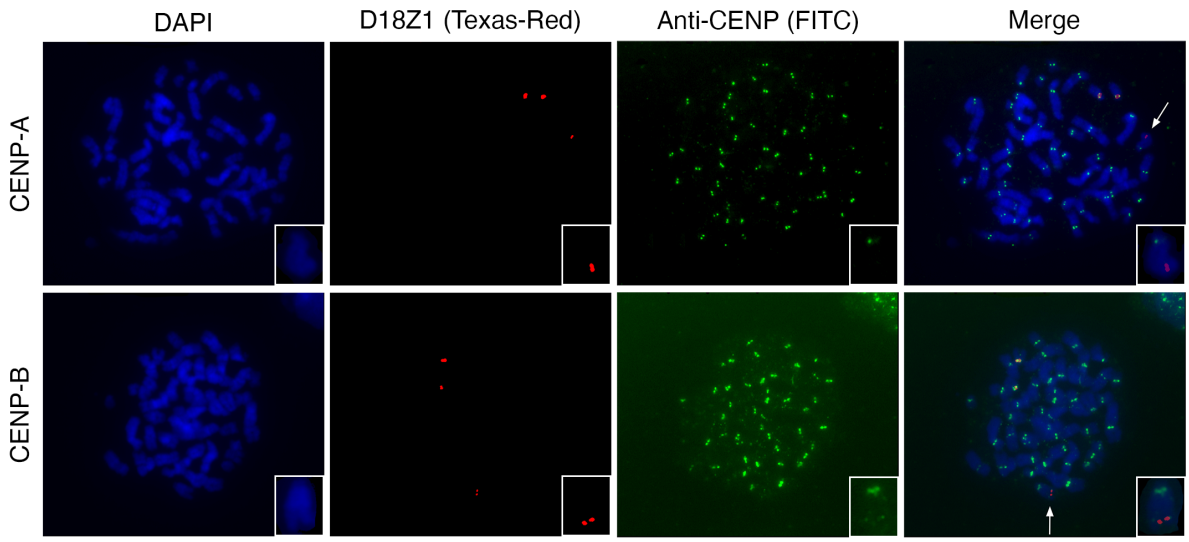

Figure 4. **CENP-A and CENP-B immuno-FISH.** Co-hybridization of the D18Z1 probe (red) with antibodies against CENP-A (*top*) and CENP-B (*bottom*) proteins (green) on chromosome metaphases from the proband. The arrows point at the derivative chromosome 15 that is also shown in larger magnification in the insets.

Discussion

During routine prenatal testing for aneuploidy by FISH, we serendipitously identified an individual carrying a *de novo* insertion of alpha satellite DNA from the centromere of chromosome 18 into cytoband 15q26 (**Figure 5**). Long-read sequencing and alignment to the CHM13-T2T genome showed that this segment transposed from a precise location of chromosome 18 centromeric HOR arrays. It also offered insights on the long-range organization of the alphoid sequence, such as homogenization of D1 monomers at positions 1 and 5.

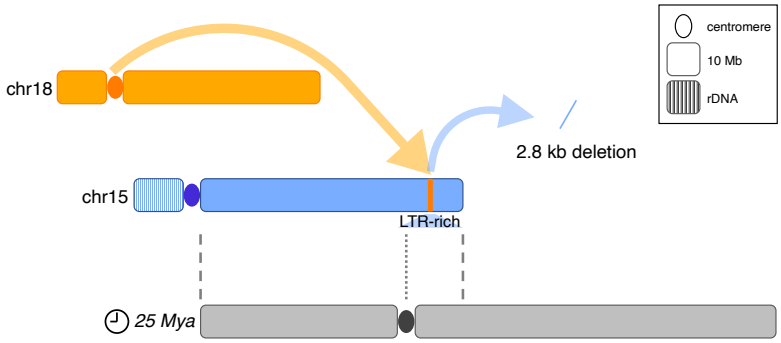

Figure 5. Schematic overview of the rearrangement. An alphoid array from the centromere of chromosome 18 inserted into an LTR-rich region of chromosome 15q26, ~10 Mbp distally from the site where an ancestral

320 centromere was seeded ~25 Mya. This transposition deleted 2.8 kbp of sequence. Dashed lines pinpoint the
321 boundaries of the synteny between chromosome 15 and the ancestral submetacentric chromosome; the dotted line
322 indicates the position of the ancestral centromere.

323

324 The lack of identification of such transposition/duplication events until now could be linked
325 either to the fact that they are extremely rare and/or because current sequencing-based
326 methodologies and analytical approaches aimed at genotyping structural variants are opaque
327 to such events due to their size and highly repetitive nature. Indeed, our standard whole-genome
328 sequencing diagnostic pipeline failed to identify this variant. Novel localizations of alphoid
329 DNA were reported in the white-cheeked gibbon, a lesser ape with an extensively rearranged
330 karyotype when compared to the ancestral primate karyotype. In this species, alpha satellite
331 DNA is found not only at centromeres but also at telomeres and interstitial positions
332 corresponding to some evolutionary breakpoints (Cellamare et al. 2009).

333 Our report brings to light a new class of structural variation that we call 'alpha satellite DNA
334 insertion' (ASI) and raises questions about the frequency, structure, mechanism, and functional
335 consequences of these events. Besides our observation, at least three additional lines of
336 evidence suggest that duplication/transposition of alphoid DNA to a new genomic location
337 occurs. First, several prenatal diagnostic reports describe the cross-hybridization of
338 chromosome-specific centromeric alpha satellite probes to heterochromatic (centromeric or
339 pericentromeric) regions of non-targeted chromosomes, i.e. the centromeres of chromosomes
340 19 and 22, the heterochromatin of chromosomes 1 and 9, and the pericentromeric region of
341 chromosome 2 (Thangavelu et al. 1998; Winsor et al. 1999; Wei et al. 2007; Musilova et al.
342 2008; Collin et al. 2009). Of note, only centromeric probes of chromosomes 18, X, and Y are
343 routinely used to screen for aneuploidies prenatally, therefore the ASI of other centromeric
344 satellites would not be found in such a serendipitous manner. Moreover, ASI smaller than the
345 standard resolution of FISH (~10 kb) would not be detected. The second line of evidence is the
346 presence of small satellite DNA blocks that are not located at centromeric or pericentromeric
347 regions in the human genome reference (Rudd and Willard 2004). While the presence of some
348 of these can be explained by the evolutionary history of the locus, like the past presence of a
349 centromere, the existence of some others may in fact be a result of fixed satellite insertion
350 events. Thirdly, the maturation process of new centromeres, i.e. epigenetic specification before
351 acquisition of the typical alpha satellite array (Kalitsis and Choo 2012; Nergadze et al. 2018),
352 *per se* implies the movement of satellite DNA to other loci.

353 Our structural characterization of the rearrangement provides some insights on the mechanism
354 of alphoid DNA spreading to non-centromeric locations. The coordinated deletion is
355 reminiscent of the mechanism inferred for duplicative transposition and suggests the
356 involvement of double-strand breakage of DNA (Cantsilieris et al. 2020), while the absence of
357 active mobile elements adjacent to the insertion or target site duplications argues against
358 retrotransposition (Deininger et al. 2003). It may be noteworthy that we also identified an
359 enrichment of LTR elements in the long-range acceptor site. LTR retrotransposon activity is
360 currently very limited or fully absent in humans (IHGSC 2001) and therefore is unlikely to
361 have directly contributed to this form of structural variation. Such repeat-rich regions have
362 been noted to be deleted as part of the duplicative transposition events associated with the new
363 insertion of large (>100 kbp) blocks of segmental duplication (Johnson et al. 2006; Cantsilieris
364 et al. 2020). Similarly, such coordinated deletions often (but not always) occur in gene-poor
365 regions of the genome minimizing functional impacts of such massive new insertions and the
366 fitness of the zygote/fetus.

367 Finally, the ASI location at 15q26 is interesting as a centromere resided at chromosome 15q25
368 in our past, ~10 Mbp away from the insertion site, and became inactive sometime between 20
369 and 25 Mya in the common ancestor of the ape lineage (Ventura et al. 2003; Giannuzzi et al.
370 2013). This observation raises the intriguing possibility that the alphoid array did not move to
371 a random repeat-rich location in the genome, but instead revisited an evolutionary favored
372 location mapping close to an ancestral centromere. Being the first observation of such events,
373 we cannot discern between these two possibilities. However, if the latter scenario is correct, it
374 might suggest that i) alphoid DNA preferentially moves to other extant or past centromeric
375 locations; ii) there are genomic loci more suitable to host the centromeric function and
376 associated alpha satellite array; iii) an alternative and opposite route to centromere
377 repositioning and new centromere formation might in fact exist, where the region first acquires
378 the satellite array and then the epigenetically-defined centromeric function emerges. Support
379 for the latter comes from the observation that introduction of alpha satellite arrays in human
380 cells can result in the formation of functional neocentromeres (Harrington et al. 1997; Ebersole
381 et al. 2000). Some observations already demonstrate that certain regions of the genome have a
382 memory and/or propensity to host centromeric function. For example, analphoid clinical new
383 centromeres are often seeded at regions corresponding to ancestral centromeres, including
384 15q24-26, the target locus of our proband (Ventura et al. 2003; Capozzi et al. 2009), or in
385 regions that are orthologous to positions that correspond to evolutionary new centromeres in

386 other primate lineages (Ventura et al. 2004; Cardone et al. 2006; Capozzi et al. 2008). Notably,
387 the seeding position frequently maps within a variable distance (~1-14 Mb) from the region
388 that hosts the centromeric function, as observed for the satellite insertion reported here. This
389 suggests that centromeric function and satellite array evolution may be restricted to region
390 rather than precise chromosomal location.

391 Besides suggesting a new class of structural variation and expanding current models of
392 centromere life cycle, this case further highlights the risk of identifying false-positive
393 aneuploidies of chromosomes 18, X, and Y when depending solely on centromeric satellite
394 probes in rapid interphase FISH. Thus, it is critically important to follow up and confirm them
395 by karyotyping. Lastly, this variant could be considered as a special case (as it occurs in the
396 euchromatin) of chromosome heteromorphism, i.e. the variation in repetitive DNA content at
397 heterochromatic regions. Although chromosome heteromorphisms are found in 2-5% of
398 individuals and are generally considered as neutral genomic variations (Tempest and Simpson
399 2017), they are associated with infertility (Sahin et al. 2008). In this regard, it is possible that
400 the aberrant presence of the alphoid array on the long arm of chromosome 15 might affect the
401 accuracy of chromosome segregation during cell division and be causative of the recurrent
402 trisomy 21 in the family. Future studies will clarify the prevalence of ASIs and their potential
403 impact on chromosome aneuploidies and infertility.

404

405 Methods

406 *Short-read sequencing and data analysis*

407 We extracted genomic DNA from cultured amniocytes of the proband using QIAamp DNA
408 mini kit (Qiagen, Hilden, Germany). We performed 150 bp paired-end WGS using the short-
409 read Illumina platform. We aligned the reads to the hg38 version of the human genome using
410 BWA-MEM version 0.7.10 (Li and Durbin 2009), run the BreakDancer version 1.4.5 (Chen et
411 al. 2009) and ERDS version 1.1 (Zhu et al. 2012), and visually inspected the 15q24-26 region
412 using the IGV tool. As we identified no structural variant, we re-aligned the reads to a custom
413 library made of chromosome 15 sequence (hg38) and a deposited sequence of alpha satellite
414 family 1 of chromosome 18 (M65181.1) (Alexandrov et al. 1991) using BWA version 0.7.17.
415 To identify read pairs mapping at the insertion breakpoints, we selected discordant pairs with
416 one end mapping on chromosome 15 and the other one on the satellite sequence and MAPQ>0.
417 We removed soft and hard clipped reads and those mapping at the pericentromeric region of

418 chromosome 15. We next identified chimeric reads spanning the breakpoints among the soft
419 clipped reads using the Integrative Genomics Viewer (IGV) tool (Robinson et al. 2011).

420

421 *Long-read sequencing and data analysis*

422 We isolated PBMC (peripheral blood mononuclear cells) from the blood of the proband and
423 both parents. We extracted DNA from approximately 1-2 million cells of actively growing
424 culture by first pelleting the cells and resuspending them in 1.0 mL Cell Lysis Solution
425 (Qiagen). The samples were incubated with RNase A solution at 37°C for 40 min. Protein
426 Precipitation Solution (Qiagen) was added at 0.33x and mixed well. After a 10 min incubation
427 on ice, the precipitate was pelleted (3 min, 15000 rpm, 4°C). The supernatant was transferred
428 to new tubes, and DNA was precipitated with an equal volume of isopropanol. The DNA was
429 pelleted (2 min, 15000 rpm, 4°C) and the pellet was washed three times with 70% EtOH. The
430 clean DNA was rehydrated with DNA Hydration Solution (Qiagen) and left for two days to
431 resuspend.

432 We generated a PacBio HiFi library from the proband's genomic DNA using g-TUBE shearing
433 (Covaris) and the Express Library Prep Kit v2 (PacBio), size selecting on the SageELF
434 platform (Sage Science) to give a tight fraction of around 23 kbp by FEMTO Pulse analysis
435 (Agilent). The library was sequenced on one SMRT Cell 8M using v2 chemistry, and we
436 obtained 20.5 Gbp of HiFi reads with mean length of 20.9 kbp and median quality of Q27. We
437 assembled the data with HiCanu (Nurk et al. 2020) and Hifiasm (Cheng et al. 2021) and aligned
438 reads to the GRCh38 (hg38) reference genome using pbmm2
439 (https://github.com/PacificBiosciences/pbmm2).

440 Adaptive sampling was performed on an ONT GridION (one flow cell per sample) using
441 readfish (Payne et al. 2020). For each sample 1.5 ug of DNA was used to prepare a LSK-109
442 library according to the manufactures protocol. DNA was sheared in a Covaris g-TUBE at 6 k
443 rpm for 2 min. The region targeted was chr15:92,309,068-92,411,920 (hg38 coordinates). ONT
444 FAST5 files were basecalled using guppy 4.0.11 using the high-accuracy model. FASTQ files
445 were pooled and aligned to hg38.no_alt.fa using both minimap2 (Li 2018) and ngmlr
446 (Sedlazeck et al. 2018). We identified reads spanning the breakpoints (located at
447 chr15:92,359,068 and chr15:92,361,920) by manual inspection of the 15q26 read alignments
448 in IGV v2.4.16 (Robinson et al. 2011). We called and phased variants using Longshot (Edge
449 and Bansal 2019) and called CpG methylation using Nanopolish (Simpson et al. 2017).

450 Selected PacBio and ONT reads were aligned to the CHM13-T2T genome using pbmm2 and
451 minimap2, respectively.

452

453 *Analysis of repeat element content*

454 We assessed the content in repeat elements in the deleted segment and in the 5 kb segments
455 upstream and downstream the insertion breakpoints by using the annotation of the GRCh38
456 RepeatMasker track (Smit et al. 2013-2015). The null distributions were generated by
457 performing 10,000 permutations of the entire 12,851 bp segment, excluding gaps and
458 centromeres, by using BEDTools version v2.30.0 (Quinlan and Hall 2010). R v4.0.3 (R Core
459 Team 2017) was used to compute empirical *P* values. Standard error (SE) was estimated using
460 the formula SE=sqrt(*P**(1-*P*)/10,000).

461

462 *Satellite monomer and HOR analysis*

463 We created a dot plot of the PacBio HiFi read 2 using the re-DOT-able tool
464 (https://www.bioinformatics.babraham.ac.uk/projects/redotable/). We extracted satellite
465 monomers from the reads containing the longest satellite sequences and anchored to the
466 proximal (PacBio HiFi read 2) or distal (ONT read 2) breakpoints by blast alignment (Altschul
467 et al. 1990) with D1 monomer sequence (AJ130751.1). We performed multiple sequence
468 alignments of monomers using Muscle (Edgar 2004) with default options. We created
469 heatmaps and plots using the gplots v3.1.0 (https://CRAN.R-project.org/package=gplots) and
470 ggplot2 v.2.2.1 (Wickham 2009) packages in the R software environment (R Core Team 2017).
471 We used the neighbor-joining method (Saitou and Nei 1987) and the Kimura 2-parameter
472 model distance (Kimura 1980), implemented in the MEGA X software (Kumar et al. 2018;
473 Stecher et al. 2020), to examine phylogenetic relationships among the satellite monomers. We
474 also included the sequences of the 12 monomer types and the alpha satellite monomer from
475 African Green Monkey as an outgroup. All ambiguous positions were removed for each
476 sequence pair (pairwise deletion option).

477

478 *FISH and Immuno-FISH*

479 FISH on uncultured amniocytes was performed with the Aquarius FAST FISH Prenatal kit
480 (Cytocell, Cambridge, UK) (DXZ1, DYZ3, D18Z1, *RB1*, *DYRK1A* probes) according to
481 manufacturer's instructions. Metaphase spreads were prepared from amniotic fluid cells and

482 lymphocytes according to standard procedures. FISH was further performed using BAC probes
483 localized in 15q25.2, RP11-752G15 (FITC) (chr15:82,627,211-82,802,988, hg38) and RP11-
484 635O8 (chr15:82,023,617-82,178,139) (TRITC) (RainbowFish, Empire Genomics, Buffalo,
485 New York, USA) and alpha-satellites probes for chromosomes 15 (D15Z1, Texas-Red), 18
486 (D18Z1, Aqua) and 13/21 (D13/21Z1, Green) (Cytocell).

487 Immuno-FISH was performed on lymphoblastoid cells from the patient. Metaphase cells
488 spreads were prepared according to a protocol adapted from Jeppesen (Jeppesen 2000). Briefly,
489 lymphoblastoid cells were harvested after 44 hour culture, incubated at 37°C with colchicine
490 (0.2µg/mL final concentration) during 2 hours, then in a 75 mM KCl hypotonic solution during
491 25 min. After centrifugation, cell pellet was resuspended in 75mM KCl/0.1% Tween20 and
492 then cytocentrifuged 5 min at 1000 rpm. The slides were transferred to a Coplin jar containing
493 KCMc solution (120 mM KCl, 20 mM NaCl, 10 mM Tris-HCl, pH 7.5, 0.5 mM EDTA, 0.1%
494 (v/v) Triton X-100) and incubated 15 min at room temperature. Then immuno-FISH was
495 performed with a protocol derived from Solovei et al. (Solovei et al. 2002) using as primary
496 antibodies mouse anti-CENP-A (Abcam, Ab13939) (1/200) and mouse anti-CENP-B (5E6C1
497 clone, generous gift from Hiroshi Masumoto, Japan) (1/200); AlexaFluor conjugated goat anti-
498 mouse as secondary antibody (1/1000) and D18Z1 probe (Texas-Red) (Cytocell). Images were
499 performed with a Zeiss AxioImager Z2 fluorescence microscope equipped with a CoolCube
500 Camera.

501

502 ## Acknowledgements

503 GG is recipient of a Pro-Women Scholarship from the Faculty of Biology and Medicine,
504 University of Lausanne. This work was supported by the Swiss National Science Foundation
505 grant 31003A_182632 and the Jérôme Lejeune Foundation to AR, by the National Institutes of
506 Health grant HG010169 to EEE, and a grant from the Brotman Baty Institute for Precision
507 Medicine to DEM and EEE. We wish to thank Emilie Chopin (Cell Biotechnology Center,
508 Hospices Civils de Lyon) for providing lymphoblastoid cell lines, as well as Patrick Lomonte
509 for his kind gift of antibodies and his advice.

510

511

References

Alexandrov IA, Mashkova TD, Akopian TA, Medvedev LI, Kisselev LL, Mitkevich SP, Yurov YB. 1991. Chromosome-specific alpha satellites: two distinct families on human chromosome 18. *Genomics* **11**: 15-23.

Altschul SF, Gish W, Miller W, Myers EW, Lipman DJ. 1990. Basic local alignment search tool. *J Mol Biol* **215**: 403-410.

Amor DJ, Choo KH. 2002. Neocentromeres: role in human disease, evolution, and centromere study. *Am J Hum Genet* **71**: 695-714.

Avarello R, Pedicini A, Caiulo A, Zuffardi O, Fraccaro M. 1992. Evidence for an ancestral alphoid domain on the long arm of human chromosome 2. *Hum Genet* **89**: 247-249.

Baldini A, Ried T, Shridhar V, Ogura K, D'Aiuto L, Rocchi M, Ward DC. 1993. An alphoid DNA sequence conserved in all human and great ape chromosomes: evidence for ancient centromeric sequences at human chromosomal regions 2q21 and 9q13. *Hum Genet* **90**: 577-583.

Cantsilieris S, Sunkin SM, Johnson ME, Anaclerio F, Huddleston J, Baker C, Dougherty ML, Underwood JG, Sulovari A, Hsieh P et al. 2020. An evolutionary driver of interspersed segmental duplications in primates. *Genome Biol* **21**: 202.

Capozzi O, Purgato S, D'Addabbo P, Archidiacono N, Battaglia P, Baroncini A, Capucci A, Stanyon R, Della Valle G, Rocchi M. 2009. Evolutionary descent of a human chromosome 6 neocentromere: a jump back to 17 million years ago. *Genome Res* **19**: 778-784.

Capozzi O, Purgato S, Verdun di Cantogno L, Grosso E, Ciccone R, Zuffardi O, Della Valle G, Rocchi M. 2008. Evolutionary and clinical neocentromeres: two faces of the same coin? *Chromosoma* **117**: 339-344.

Cardone MF, Alonso A, Pazienza M, Ventura M, Montemurro G, Carbone L, de Jong PJ, Stanyon R, D'Addabbo P, Archidiacono N et al. 2006. Independent centromere formation in a capricious, gene-free domain of chromosome 13q21 in Old World monkeys and pigs. *Genome Biol* **7**: R91.

Cellamare A, Catacchio CR, Alkan C, Giannuzzi G, Antonacci F, Cardone MF, Della Valle G, Malig M, Rocchi M, Eichler EE et al. 2009. New insights into centromere organization and evolution from the white-cheeked gibbon and marmoset. *Mol Biol Evol* **26**: 1889-1900.

Chen K, Wallis JW, McLellan MD, Larson DE, Kalicki JM, Pohl CS, McGrath SD, Wendl MC, Zhang Q, Locke DP et al. 2009. BreakDancer: an algorithm for high-resolution mapping of genomic structural variation. *Nat Methods* **6**: 677-681.

Cheng H, Concepcion GT, Feng X, Zhang H, Li H. 2021. Haplotype-resolved de novo assembly using phased assembly graphs with hifiasm. *Nat Methods* **18**: 170-175.

Chiatante G, Giannuzzi G, Calabrese FM, Eichler EE, Ventura M. 2017. Centromere Destiny in Dicentric Chromosomes: New Insights from the Evolution of Human Chromosome 2 Ancestral Centromeric Region. *Mol Biol Evol* **34**: 1669-1681.

Collin A, Sladkevicius P, Soller M. 2009. False-positive prenatal diagnosis of trisomy 18 by interphase FISH: hybridization of chromosome 18 alpha-satellite probe (D18Z1) to chromosome 2. *Prenat Diagn* **29**: 1279-1281.

Deininger PL, Moran JV, Batzer MA, Kazazian HH, Jr. 2003. Mobile elements and mammalian genome evolution. *Curr Opin Genet Dev* **13**: 651-658.

Durfy SJ, Willard HF. 1989. Patterns of intra- and interarray sequence variation in alpha satellite from the human X chromosome: evidence for short-range homogenization of tandemly repeated DNA sequences. *Genomics* **5**: 810-821.

Earnshaw WC, Migeon BR. 1985. Three related centromere proteins are absent from the inactive centromere of a stable isodicentric chromosome. *Chromosoma* **92**: 290-296.

Ebersole TA, Ross A, Clark E, McGill N, Schindelhauer D, Cooke H, Grimes B. 2000. Mammalian artificial chromosome formation from circular alphoid input DNA does not require telomere repeats. *Hum Mol Genet* **9**: 1623-1631.

Edgar RC. 2004. MUSCLE: multiple sequence alignment with high accuracy and high throughput. *Nucleic Acids Res* **32**: 1792-1797.

Edge P, Bansal V. 2019. Longshot enables accurate variant calling in diploid genomes from single-molecule long read sequencing. *Nat Commun* **10**: 4660.

Feliciello I, Pezer Z, Kordis D, Bruvo Madaric B, Ugarkovic D. 2020. Evolutionary History of Alpha Satellite DNA Repeats Dispersed within Human Genome Euchromatin. *Genome Biol Evol* **12**: 2125-2138.

Giannuzzi G, Pazienza M, Huddleston J, Antonacci F, Malig M, Vives L, Eichler EE, Ventura M. 2013. Hominoid fission of chromosome 14/15 and the role of segmental duplications. *Genome Res* **23**: 1763-1773.

Harrington JJ, Van Bokkelen G, Mays RW, Gustashaw K, Willard HF. 1997. Formation of de novo centromeres and construction of first-generation human artificial microchromosomes. *Nat Genet* **15**: 345-355.

IHGSC. 2001. Initial sequencing and analysis of the human genome. *Nature* **409**: 860-921.

IJdo JW, Baldini A, Ward DC, Reeders ST, Wells RA. 1991. Origin of human chromosome 2: an ancestral telomere-telomere fusion. *Proc Natl Acad Sci U S A* **88**: 9051-9055.

Jeppesen P. 2000. Immunofluorescence in cytogenetic analysis: method and applications. *Genetics and Molecular Biology* **23**: 1003-1014.

Johnson ME, National Institute of Health Intramural Sequencing Center Comparative Sequencing P, Cheng Z, Morrison VA, Scherer S, Ventura M, Gibbs RA, Green ED, Eichler EE. 2006. Recurrent duplication-driven transposition of DNA during hominoid evolution. *Proc Natl Acad Sci U S A* **103**: 17626-17631.

Kalitsis P, Choo KH. 2012. The evolutionary life cycle of the resilient centromere. *Chromosoma* **121**: 327-340.

Karpen GH, Allshire RC. 1997. The case for epigenetic effects on centromere identity and function. *Trends Genet* **13**: 489-496.

Kimura M. 1980. A simple method for estimating evolutionary rates of base substitutions through comparative studies of nucleotide sequences. *J Mol Evol* **16**: 111-120.

Kumar S, Stecher G, Li M, Knyaz C, Tamura K. 2018. MEGA X: Molecular Evolutionary Genetics Analysis across Computing Platforms. *Mol Biol Evol* **35**: 1547-1549.

Li H. 2018. Minimap2: pairwise alignment for nucleotide sequences. *Bioinformatics* **34**: 3094-3100.

Li H, Durbin R. 2009. Fast and accurate short read alignment with Burrows-Wheeler transform. *Bioinformatics* **25**: 1754-1760.

Logsdon GA, Vollger MR, Hsieh P, Mao Y, Liskovykh MA, Koren S, Nurk S, Mercuri L, Dishuck PC, Rhie A et al. 2020. The structure, function, and evolution of a complete human chromosome 8. *bioRxiv* doi:10.1101/2020.09.08.285395: 2020.2009.2008.285395.

Loose M, Malla S, Stout M. 2016. Real-time selective sequencing using nanopore technology. *Nat Methods* **13**: 751-754.

Marshall OJ, Chueh AC, Wong LH, Choo KH. 2008. Neocentromeres: new insights into centromere structure, disease development, and karyotype evolution. *Am J Hum Genet* **82**: 261-282.

McKinley KL, Cheeseman IM. 2016. The molecular basis for centromere identity and function. *Nat Rev Mol Cell Biol* **17**: 16-29.

McNulty SM, Sullivan BA. 2018. Alpha satellite DNA biology: finding function in the recesses of the genome. *Chromosome Res* **26**: 115-138.

Miga KH, Koren S, Rhie A, Vollger MR, Gershman A, Bzikadze A, Brooks S, Howe E, Porubsky D, Logsdon GA et al. 2020. Telomere-to-telomere assembly of a complete human X chromosome. *Nature* **585**: 79-84.

Miga KH, Newton Y, Jain M, Altemose N, Willard HF, Kent WJ. 2014. Centromere reference models for human chromosomes X and Y satellite arrays. *Genome Res* **24**: 697-707.

Montefalcone G, Tempesta S, Rocchi M, Archidiacono N. 1999. Centromere repositioning. *Genome Res* **9**: 1184-1188.

Musilova P, Rybar R, Oracova E, Vesela K, Rubes J. 2008. Hybridization of the 18 alpha-satellite probe to chromosome 1 revealed in PGD. *Reprod Biomed Online* **17**: 695-698.

Nergadze SG, Piras FM, Gamba R, Corbo M, Cerutti F, McCarter JGW, Cappelletti E, Gozzo F, Harman RM, Antczak DF et al. 2018. Birth, evolution, and transmission of satellite-free mammalian centromeric domains. *Genome Res* **28**: 789-799.

Nurk S, Walenz BP, Rhie A, Vollger MR, Logsdon GA, Grothe R, Miga KH, Eichler EE, Phillippy AM, Koren S. 2020. HiCanu: accurate assembly of segmental duplications, satellites, and allelic variants from high-fidelity long reads. *Genome Res* **30**: 1291-1305.

620 Otake K, Ohzeki JI, Shono N, Kugou K, Okazaki K, Nagase T, Yamakawa H, Kouprina N, Larionov
621 V, Kimura H et al. 2020. CENP-B creates alternative epigenetic chromatin states permissive
622 for CENP-A or heterochromatin assembly. *J Cell Sci* **133**.
623 Palmer DK, O'Day K, Trong HL, Charbonneau H, Margolis RL. 1991. Purification of the centromere-
624 specific protein CENP-A and demonstration that it is a distinctive histone. *Proc Natl Acad Sci*
625 *U S A* **88**: 3734-3738.
626 Panchenko T, Black BE. 2009. The epigenetic basis for centromere identity. *Prog Mol Subcell Biol* **48**:
627 1-32.
628 Payne A, Holmes N, Clarke T, Munro R, Debebe BJ, Loose M. 2020. Readfish enables targeted
629 nanopore sequencing of gigabase-sized genomes. *Nat Biotechnol* doi:10.1038/s41587-020-
630 00746-x.
631 Piras FM, Nergadze SG, Magnani E, Bertoni L, Attolini C, Khoriauli L, Raimondi E, Giulotto E. 2010.
632 Uncoupling of satellite DNA and centromeric function in the genus Equus. *PLoS Genet* **6**:
633 e1000845.
634 Quinlan AR, Hall IM. 2010. BEDTools: a flexible suite of utilities for comparing genomic features.
635 *Bioinformatics* **26**: 841-842.
636 R Core Team. 2017. R: A language and environment for statistical computing., https://www.r-
637 project.org/.
638 Robinson JT, Thorvaldsdottir H, Winckler W, Guttman M, Lander ES, Getz G, Mesirov JP. 2011.
639 Integrative genomics viewer. *Nat Biotechnol* **29**: 24-26.
640 Rocchi M, Stanyon R, Archidiacono N. 2009. Evolutionary new centromeres in primates. *Prog Mol*
641 *Subcell Biol* **48**: 103-152.
642 Rosenbloom KR, Armstrong J, Barber GP, Casper J, Clawson H, Diekhans M, Dreszer TR, Fujita PA,
643 Guruvadoo L, Haeussler M et al. 2015. The UCSC Genome Browser database: 2015 update.
644 *Nucleic Acids Res* **43**: D670-681.
645 Rudd MK, Willard HF. 2004. Analysis of the centromeric regions of the human genome assembly.
646 *Trends Genet* **20**: 529-533.
647 Sahin FI, Yilmaz Z, Yuregir OO, Bulakbasi T, Ozer O, Zeyneloglu HB. 2008. Chromosome
648 heteromorphisms: an impact on infertility. *J Assist Reprod Genet* **25**: 191-195.
649 Saitou N, Nei M. 1987. The neighbor-joining method: a new method for reconstructing phylogenetic
650 trees. *Mol Biol Evol* **4**: 406-425.
651 Schueler MG, Higgins AW, Rudd MK, Gustashaw K, Willard HF. 2001. Genomic and genetic
652 definition of a functional human centromere. *Science* **294**: 109-115.
653 Sedlazeck FJ, Rescheneder P, Smolka M, Fang H, Nattestad M, von Haeseler A, Schatz MC. 2018.
654 Accurate detection of complex structural variations using single-molecule sequencing. *Nat*
655 *Methods* **15**: 461-468.
656 Simpson JT, Workman RE, Zuzarte PC, David M, Dursi LJ, Timp W. 2017. Detecting DNA cytosine
657 methylation using nanopore sequencing. *Nat Methods* **14**: 407-410.
658 Smit AFA, Hubley R, Green P. 2013-2015. RepeatMasker Open-4.0.
659 Solovei I, Cavallo A, Schermelleh L, Jaunin F, Scasselati C, Cmarko D, Cremer C, Fakan S, Cremer T.
660 2002. Spatial preservation of nuclear chromatin architecture during three-dimensional
661 fluorescence in situ hybridization (3D-FISH). *Exp Cell Res* **276**: 10-23.
662 Stecher G, Tamura K, Kumar S. 2020. Molecular Evolutionary Genetics Analysis (MEGA) for macOS.
663 *Mol Biol Evol* **37**: 1237-1239.
664 Tempest HG, Simpson JL. 2017. Why are we still talking about chromosomal heteromorphisms?
665 *Reprod Biomed Online* **35**: 1-2.
666 Thangavelu M, Chen PX, Pergament E. 1998. Hybridization of chromosome 18 alpha-satellite DNA
667 probe to chromosome 22. *Prenat Diagn* **18**: 922-925.
668 Ventura M, Mudge JM, Palumbo V, Burn S, Blennow E, Pierluigi M, Giorda R, Zuffardi O,
669 Archidiacono N, Jackson MS et al. 2003. Neocentromeres in 15q24-26 map to duplicons which
670 flanked an ancestral centromere in 15q25. *Genome Res* **13**: 2059-2068.
671 Ventura M, Weigl S, Carbone L, Cardone MF, Misceo D, Teti M, D'Addabbo P, Wandall A, Bjorck E,
672 de Jong PJ et al. 2004. Recurrent sites for new centromere seeding. *Genome Res* **14**: 1696-1703.

673 Voullaire LE, Slater HR, Petrovic V, Choo KH. 1993. A functional marker centromere with no
674 detectable alpha-satellite, satellite III, or CENP-B protein: activation of a latent centromere?
675 *Am J Hum Genet* **52**: 1153-1163.
676 Wei S, Siu VM, Decker A, Quigg MH, Roberson J, Xu J, Adeyinka A. 2007. False-positive prenatal
677 diagnosis of trisomy 18 by interphase FISH: hybridization of chromosome 18 alpha-satellite
678 DNA probe (D18Z1) to the heterochromatic region of chromosome 9. *Prenat Diagn* **27**: 1064-
679 1066.
680 Wickham H. 2009. *ggplot2: Elegant Graphics for Data Analysis*. Springer-Verlag New York.
681 Willard HF, Waye JS. 1987. Hierarchical order in chromosome-specific human alpha satellite DNA.
682 *Trends in Genetics* **3**: 192-198.
683 Winsor EJ, Dyack S, Wood-Burgess EM, Ryan G. 1999. Risk of false-positive prenatal diagnosis using
684 interphase FISH testing: hybridization of alpha-satellite X probe to chromosome 19. *Prenat*
685 *Diagn* **19**: 832-836.
686 Zhu M, Need AC, Han Y, Ge D, Maia JM, Zhu Q, Heinzen EL, Cirulli ET, Pelak K, He M et al. 2012.
687 Using ERDS to infer copy-number variants in high-coverage genomes. *Am J Hum Genet* **91**:
688 408-421.

689